Planetary Nebulae: Multi-Wavelength Probes of Stellar and Galactic Evolution
Proceedings IAU Symposium No. 323, 2016
X. Liu, L. Stanghellini & A. Karakas, eds.

doi:10.1017/S1743921317001971

Herschel observations of planetary nebulae†

Griet C. Van de Steene

Royal Observatory of Belgium, Department Astronomy and Astrophysics
Ringlaan 3, BE-1180, Brussels, Belgium
email: g.vandesteene@oma.be

Abstract. This article presents an overview of the published results for planetary nebulae based on images and spectroscopy from the PACS, SPIRE, and HIFI instruments on board the Herschel satellite.

Keywords. ISM: abundances, atoms, dust, globules, molecules, planetary nebulae: general, infrared: ISM, stars: circumstellar matter

1. Introduction

Grains play an important role in many environments, including planetary nebulae (PNe), because of extinction, photoelectric heating, their influence on the charge and ionization balance of the gas, as catalysts for grain-surface chemical reactions and as seeds for freeze-out of molecules. Previous satellite missions such as IRAS, ISO, Spitzer, and AKARI have allowed us to study the dust in PNe, but unfortunately the angular resolution of these instruments was too low to get detailed information on the spatial distribution of the dust. This has changed with the Herschel satellite, which has allowed us to study the spatial structures in unprecedented detail.

2. Herschel and its instruments

The Herschel Space Observatory (Pilbratt *et al.* 2010) was launched on May 14 2009 and operated for nearly four years. It carried the largest, most powerful infrared telescope ever flown in space and three sensitive scientific instruments. Herschel's observations finished on April 29 2014 when the tank of liquid helium used to cool the instruments finally ran dry.

The three instruments on board were: PACS (Photoconductor Array Camera and Spectrometer), SPIRE (Spectral and Photometric Imaging REceiver), and HIFI (Heterodyne Instrument for the Far Infrared), a high-resolution spectrometer. These instruments were designed for deep, wideband photometry with high spatial resolution and full spectral coverage, making Herschel the first space facility to completely cover the far infrared and submillimeter range from 55 to 672 μm.

PACS (Photodetecting Array Camera and Spectrometer) (Poglitsch *et al.* 2010) was an imaging camera and low-resolution spectrometer covering wavelengths from 55 to 210 μm. The spectrometer had a spectral resolution between R = 1000 and R = 5000. It operated as an integral field spectrograph, combining spatial and spectral resolution. The imaging camera was able to image simultaneously in two bands (either 60 − 85 / 85 − 130 μm and 130 − 210 μm) with a detection limit of a few mJy.

† *Herschel* is an ESA space observatory with science instruments provided by European-led Principal Investigator consortia and with important participation from NASA.

SPIRE (Spectral and Photometric Imaging Receiver) (Griffin *et al.* 2010) was an imaging camera and low-resolution spectrometer covering 194 to 672 μm wavelength. The spectrometer had a resolution between R = 40 and R = 1000 at a wavelength of 250 μm and was able to image point sources with brightnesses around 100 mJy and extended sources with brightnesses of around 500 mJy. The imaging camera observed simultaneously in three bands, centred at 250, 350 and 500 μm, each with 139, 88 and 43 pixels respectively. It was able to detect point sources with brightness above 2 mJy.

HIFI (Heterodyne Instrument for the Far Infrared) (de Grauw *et al.* 2010) is a heterodyne detector able to electronically separate radiation of different wavelengths, giving a spectral resolution up to $R = 10^7$. The spectrometer was operated within two wavelength bands, from 157 to 212 μm and from 240 to 625 μm.

3. PACS and SPIRE imaging results

The extended circumstellar envelopes of evolved low-mass AGB stars display a large variety of morphologies. Understanding the various mechanisms that give rise to these extended structures is important to trace their mass-loss history. The data presented by Cox *et al.* (2012) showed for the first time the variety of interaction between the circumstellar shell and the interstellar medium, which can be divided in roughly four categories: "fermata", "eyes", "irregular", and "rings". In particular the star's peculiar space velocity and the density of the ISM appear decisive in detecting emission from bow shocks or detached rings. Tentatively, the "eyes" class objects are associated with (visual) binaries, while the "rings" generally do not appear to occur for M-type stars, only for C or S-type objects that have experienced a thermal pulse. The occurrence of the observed eye-shape of AGB detached shells is most strongly influenced by the interstellar magnetic field, the stellar space motion, and density of the interstellar medium (van Marle *et al.* 2014). Observability of this transient phase is favoured for lines-of-sight perpendicular to the interstellar magnetic field direction. The simulations of van Marle *et al.* (2014) indicate that "eye" shapes of such pre-PN circumstellar shells can strongly affect the shape and size of PNe.

A total of 18 well known PNe have been imaged with PACS and SPIRE instruments in the framework of MESS and HerPlans programs. Seven PNe (NGC 6720, NGC 650, NGC 7293, NGC 6853, NGC 3587, NGC 7027) were imaged by the MESS team. Mass loss of Evolved StarS (MESS) was a Guarenteed Time Key Programme to study the circumstellar environment of evolved post main sequence stars. A detailed description of the program can be found in Groenewegen *et al.* (2011). An overview of the Herschel observations of PNe in the MESS program was presented in van Hoof *et al.* (2012). Eleven PNe (NGC 40, NGC 2392, NGC 3242, NGC 6445, NGC 6543, NGC 6720, NGC 6781, NGC 6826, NGC 7009, NGC 7026, Mz 3) have been observed in the Herschel Planetary Nebulae Survey (HerPlanS). A data overview and first analysis was presented in Ueta *et al.* (2014). HerPlaNS obtained far-infrared broadband images and spectra of eleven well-known PNe with the PACS and SPIRE instruments. The target PNe all have distances less than ∼1.5 kpc and are dominated by relatively high-excitation nebulae as they were selected from the Chandra Planetary Nebula Survey (ChanPlaNS; Kastner *et al.* 2012)

Herschel PACS and SPIRE imaging showed that the dust emission in PNe has a very clumpy structure for all nebula. There is excellent agreement between the H_2 images and the PACS 70 μm maps. For the Ring nebula (NGC 6720, Figure 1) it appears to be the first observational evidence that H_2 forms on oxygen rich dust grains. van Hoof *et al.* (2010) developed a photoionisation model of the Ring nebula with `Cloudy` to investigate

https://doi.org/10.1017/S1743921317001971 Published online by Cambridge University Press

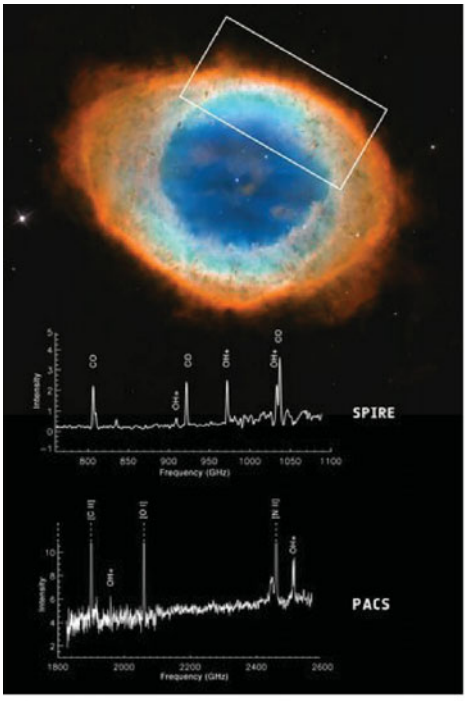

(a) SPIRE and PACS spectra of molecules in the Ring nebula NGC 6720.

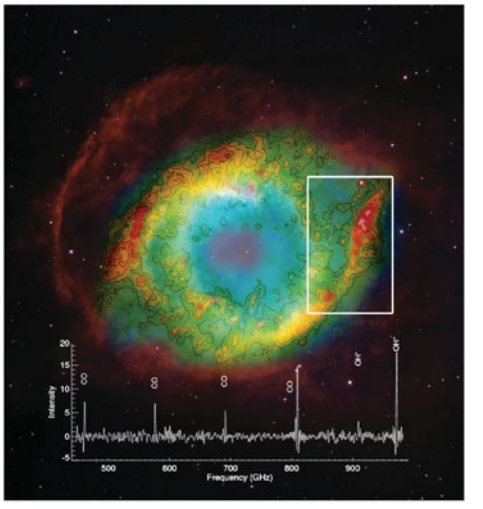

(b) SPIRE 250 μm image and spectrum of molecules in the Helix nebula NGC 7293.

Figure 1. Herschel spectra of molecules in the Ring and Helix nebula

possible formation scenarios for H_2. They concluded that the most plausible scenario is that the H_2 resides in high density knots which were formed after the recombination of the gas started, when the central star luminosity dropped steeply after the central star entered the cooling track. H_2 formation may still be ongoing at this moment, depending on the density of the knots and the properties of the grains in the knots (van Hoof *et al.* 2010). This is also a possible scenario for the formation of high density clumps in other evolved nebula with a central star on the cooling track such as the Helix (NGC 7293, Figure 1) and the Dumbell (NGC 6853).

Comparison between the 70 μm Herschel and corresponding optical maps showed that they are very similar indicating that there is a very steep temperature gradient from the ionized region to the dusty photodissociation region. For NGC 6781 the PACS 70 μm map, showing the distribution of thermal dust continuum is very similar to what is seen in the [NII]λ658.4 nm image (Ueta *et al.* 2014). For the Helix it was also observed and shown that the radiation field decreases rapidly outwards through the barrel wall (Fig. 9, Van de Steene *et al.* 2015).

Previous knowledge of the 3D structure of the nebula is extremely useful to correctly interpret the far infrared images. For instance, the PACS and SPIRE images of the Helix nebula could be understood based on the kinematic model of Zeigler *et al.* (2013) and the Herschel images of NGC 6781 with the 3D model of Schwarz & Monteiro (2006). Both show bipolar, barrel-like structures inclined to the line of sight, a frequent morphology in PNe.

Herschel PACS imaging photometry was obtained for these 17 different PNe in the MESS and HerPlanS projects (van Hoof *et al.* 2010, van Hoof *et al.* 2013, Van de Steene

https://doi.org/10.1017/S1743921317001971 Published online by Cambridge University Press

et al. 2015,Van de Steene *et al.* in preparation, Ueta *et al.* 2014, Ueta *et al.* in preparation) with the PACS and SPIRE instruments at 70, 160, 250, 350, and 500 μm. This photometry was complemented with photometry obtained from the literature at many other wavelengths from the UV to radio wavelengths to construct full SEDs. The modified black body fit to these SEDs revealed that the emission factor β is always close to 1.0, indicating that the dust grains are mainly amorphous carbon (Menella *et al.* 1995, Boudet *et al.* 2005). The fit to the SED also showed that the flux emitted in the far infrared is significant: without far-IR data fitting constraints the dust mass is underestimated by 40%.

The dust temperature obtained from the SED fits and the temperature maps made, showed that the cool dust temperature of the PNe is around 30 to 100 K. For the Helix nebula the gas kinetic temperature T_k was determined to be about 20 to 40 K (Zack & Ziurys 2013, Etxaluze *et al.* 2014), which is similar the Helix' dust temperature (Van de Steene *et al.* 2015). The gas density of the H_2 cometary globules is on the order of $n(H_2) \sim (1\text{-}5)\,10^5\,cm^{-3}$. Goldsmith (2001) found that for gas densities higher than $10^{4.5}\,cm^{-3}$ the dust and gas temperatures will be closely coupled, also for the dust temperatures determined for the Helix nebula.

The dust masses found so far for NGC 6781, NGC 7293, and NGC 650 are all a few thousandths of solar masses. By integrating over the entire nebula, the dust column mass density map the total mass of far emitting dust mass was determined to be $4 \times 10^{-3}\,M_\odot$ for NGC 6781 at a distance of 950 pc and $3.5 \times 10^{-3}\,M_\odot$ for the Helix nebula at distance of 216 pc, while for NGC 650 the dust mass is about $1.4 \times 10^{-3}\,M_\odot$ at a distance of 1200 pc based on Cloudy modeling (Ueta *et al.* 2014, Van de Steene *et al.* 2015, van Hoof *et al.* 2013)

One of the goals of HerPlaNS is to empirically obtain spatially resolved gas-to-dust mass ratio distribution maps by deriving both the dust and gas column mass distribution maps directly from observational data. For NGC 6781 direct comparison of the dust and gas column mass maps constrained data allowed to construct an empirical gas-to-dust mass ratio map, which showed a large range of ratios with the median of 195±110 and hence, is generally consistent with the typical spatially-unresolved ratio between 100 and 400 widely used in the literature for the case of PNe and AGB stars (Ueta *et al.* 2014).

The MESS and HerPlaNS teams have collected not only photometry, but also other spectroscopic data from the literature over the whole spectral range from X-rays to radio to make the most comprehensive Cloudy models ever made of NGC 650 (van Hoof *et al.* 2013) and NGC 6781 (M. Otsuki, this volume). For NGC 650 the `Cloudy` model showed that the grains in the ionized nebula are large (assuming single-sized grains, they would have a radius of 0.15 μm). Most likely these large grains were inherited from the asymptotic giant branch phase. However the PACS 70/160 μm temperature map showed evidence of two radiation components heating the grains. The first component is direct emission from the central star, while the second component is diffuse emission from the ionized gas (mainly Lyα). Unlike what was thought before, the neutral material resides in dense clumps inside the ionized region. These may also harbour stochastically heated very small grains in addition to the large grains. This is unusual for such a highly evolved PN.

In the past, far-IR SED fitting with broadband fluxes were performed under the assumption of negligible line contamination. With the Herschel data and `Cloudy` modeling we verified that the degree of line contamination is approximately 8-20% (Ueta *et al.* 2014, van Hoof *et al.* 2013) and does not significantly affect the fitting results.

https://doi.org/10.1017/S1743921317001971 Published online by Cambridge University Press

4. PACS and SPIRE spectroscopic results

4.1. *NGC 6781*

The Herschel spectra obtained at various locations within NGC 6781 revealed both the physical and chemical nature of the nebula. The spectra showed a number of ionic and atomic lines such as [O III] 52, 88 μm, [N III] 57 μm, [N II] 122, 205 μm, [C II] 158 μm, and [O I] 63, 146 μm, as well as various molecular lines, in particular, high-J CO rotational transitions, OH, and OH^+ emission lines. Thermal dust continuum emission was also detected in most bands in these deep exposure spectra. On average, the relative distributions of emission lines of various nature suggested that the barrel cavity in NGC 6781 is uniformly highly ionized, with a region of lower ionization delineating the inner surface of the barrel wall. The least ionic and atomic gas, molecular, and dust species are concentrated in the cylindrical barrel structure.

Based on the PACS IFU spectral cube data, Ueta *et al.* (2014) derived line maps in the detected ionic and atomic fine-structure lines. Next diagnostics of the electron temperature and density using line ratios such as [O III] 52/88 μm and [N II] 122/205 μm, resulted in (T_e, n_e) and ionic/elemental/relative abundance profiles for the first time in the far-IR for any PN. The derived T_e profile substantiated the typical assumption of uniform $T_e = 10^4$K in the main ionized region, while showing an interesting increase in the barrel (up to 10% higher), followed by a sudden tapering off toward the halo region. The n_e profile of high-excitation species is nearly flat across the inner cavity of the nebula, whereas the n_e profile of low excitation species exhibits a radially increasing tendency with a somewhat complex variation around the barrel wall. In fact, this n_e[N II] profile is reflected in the physical stratification of the nebula revealed by the ionic/elemental abundance analysis. The detected stratification is consistent with the previous inferences made from the past optical imaging observations in various emission lines of varying levels of excitation. The derived relative elemental abundance profiles showed uniformly low N and C abundances, confirming the low initial mass (< 2 $M_\odot$) and marginally carbon-rich nature of the central star. However, the profiles did not appear to reveal variations reflecting the evolutionary change of the central star, such as a radially increasing carbon abundance.

4.2. *SPIRE spectroscopy: OH^+ and CO*

Etxaluze *et al.* (2014) and Aleman *et al.* (2014) reported the first detection of extended OH^+ lines in emission in 5 PNe observed as part of the HerPlans in NGC 6445, NGC 6720 (Fig. 1a), and NGC 6781 and MESS in NGC 7293 (Fig. 1b). Also NGC 6853 shows OH^+ in emission (Van de Steene *et al.*, in preparation). All five PNe are molecule rich, with dense clumpy structures and hot central stars (Teff $>$ 100000 K). The OH^+ emission is most likely due to excitation in a photodissociation region. Although other factors such as high density and low C/O ratio may also play a role in the enhancement of the OH^+ emission. The fact that OH^+ is not detected in objects with $T_{eff} < 100000$ K suggests that the hardness of the ionising central star spectra could be an important factor in the production of OH^+ emission in PNe.

The Herschel spectra towards the Helix nebula also show, besides OH^+, CO emission lines (from J = 4 to 8), [N II] at 1461 GHz from ionized gas, and [C I] ($^3P_2 - ^3P_1$). The SPIRE spectral maps suggest that CO arises from dense and shielded clumps in the western rims of the Helix nebula, whereas OH^+ and [C I] lines trace the diffuse gas and the UV and X-ray illuminated clump surfaces where molecules reform after CO photodissociation. The [N II] line traces a more diffuse ionized gas component in the interclump medium (Etxaluze *et al.* 2014).

https://doi.org/10.1017/S1743921317001971 Published online by Cambridge University Press

For NGC 6781 the CO observations and analysis with higher-J transitions sampled a much warmer CO gas component in the cylindrical barrel structure, probably located closer to the equatorial region along the line of sight, compared with the previous CO measurements and diagnostics by Bachiller *et al.* (1993). However, the amount of this warm component was determined to be an order of magnitude smaller than the cold component (Ueta *et al.* 2014).

4.3. *Crystalline olivine*

Blommaert *at al.* (2014) (GT1 "Forsterite dust in the circumstellar environment of evolved stars") presented 48 PACS spectra of evolved stars in the wavelength range of $67-72\ \mu$m, covering the $69\ \mu$m band of crystalline olivine ($Mg_{22x}Fe_{(2x)}SiO_4$). For 27 objects in the sample, they detected the $69\ \mu$m band of crystalline olivine ($Mg_{(22x)}Fe_{(2x)}SiO_4$). The $69\ \mu$m band showed that all the sources produce pure forsterite grains containing no iron in their lattice structure. They fit the $69\ \mu$m band and used its width and wavelength position to probe the composition and temperature of the crystalline olivine. The fits showed that on average the temperature of the crystalline olivine is highest in the group of OH/IR stars and the post-AGB stars with confirmed Keplerian disks. The temperature is lower for the other post-AGB stars and lowest for the PNe. A couple of the detected $69\ \mu$m bands are broader than those of pure magnesium-rich crystalline olivine, which can be due to a temperature gradient in the circumstellar environment of these stars.

5. HIFI

5.1. *HIFISTARS*

The Herschel guaranteed time key programme HIFISTARS (Bujarrabal *et al.* 2012) aimed to study the physical conditions, particularly the excitation state, of the intermediate-temperature gas in proto-PNe and young PNe. The information that the observations of the different components deliver is of particular importance for the wind-shock interaction and hence understanding the evolution and shaping of PNe. They performed Herschel/HIFI observations of intermediate-excitation molecular lines in the far-infrared range of a sample of ten nebulae. The high spectral resolution provided by HIFI allows the accurate measurement of the line profiles. The dynamics and evolution of these nebulae are known to result from the presence of several gas components, notably fast bipolar outflows and slow shells (that often are the fossil AGB shells), and the interaction between them. Because of the diverse kinematic properties of the different components, their emission can be identified in the line profiles. The observation of these high-energy transitions allows an accurate study of the excitation conditions, particularly in the warm gas, which cannot be properly studied from the low-energy lines. They detected far infrared lines of several molecules, in particular of ^{12}CO, ^{13}CO, and H_2O. Emission from other species, like NH_3, OH, $H_2{}^{18}O$, HCN, SiO, etc., has been also detected. Wide profiles showing sometimes spectacular line wings have been found. In the case of CRL 618 the ^{12}CO and ^{13}CO high excitation line profiles present a composite structure showing spectacular wings in some cases, which become dominant as the energy level increases (Soria-Ruiz *et al.* 2013). Bujarrabal *et al.* (2012) mainly studied the excitation properties of the high-velocity emission, which is known to come from fast bipolar outflows. From comparison with general theoretical predictions, they find that CRL 618 showed a particularly warm fast wind $\sim$300 K, hotter than previously estimated (Soria-Ruiz *et al.* 2013). In contrast, the fast winds in OH 231.8+4.2 and NGC 6302 are cold, $T_k \sim 30$ K.

https://doi.org/10.1017/S1743921317001971 Published online by Cambridge University Press

Other nebulae, like CRL 2688, show intermediate temperatures, with characteristic values around 100 K. They argue that the differences in temperature in the different nebulae can be caused by cooling after the gas acceleration (that is probably caused by shocks). For instance, CRL 618 is a case of very recent acceleration of the gas by shocks, less than ∼100 yr ago, while the fast gas in OH 231.8+4.2 was accelerated ∼1000 yr ago. They also find indications that the densest gas tends to be cooler, which may be explained by the expected increase of the radiative cooling efficiency with density. The dense central core of CRL 618 is characterised by a very low expansion velocity, $\sim 5\,\mathrm{km\,s^{-1}}$, and a strong velocity gradient. This component is very likely to be the unaltered circumstellar layers that are lost in the last AGB phase, where the ejection velocity is particularly low. The physical properties of the diffuse halo and the double empty shell, contribute to its line profiles mainly in the low-J CO transitions (Soria-Ruiz *et al.* 2013).

5.2. *Shapemol*

Herschel/HIFI has opened a new window for probing molecular warm gas. On the other hand, the software `SHAPE` (Steffen & Lopez 2006, Steffen *et al.* 2011) has emerged in the past few years as a standard tool for determining the morphology and velocity field of different kinds of gaseous emission nebulae via spatio-kinematical modelling. `SHAPE` implements radiative transfer solving, but it is only available for atomic species and not for molecules. SHAPEMOL (Santander-Garcia *et al.* 2015) is a complement to `SHAPE` which enables user-friendly, spatio-kinematic modelling with accurate non-LTE calculations of excitation and radiative transfer in CO lines. `Shapemol` is a plug-in completely integrated within `SHAPE v5` . It allows radiative transfer solving in the ^{12}CO and ^{13}CO J =10 to J = 1716 lines, but its implementation easily permits extending the code to different transitions and other molecular species, either by the code developers or by the user. Used along `Shape`, `Shapemol` allows easily generating synthetic maps and synthetic line profiles to match against observations.

As an example of the power and versatility of `Shapemol`, a model of the molecular envelope of the planetary nebula NGC 6302 was made and compared with ^{12}CO and ^{13}CO J = 21 interferometric maps from SMA and high-J transitions from HIFI. Santander-Garcia *et al.* (2015) found that its molecular envelope has a complex, broken ring-like structure with an inner, hotter region and several fingers and high-velocity blobs, emerging outwards from the plane of the ring. The Herschel spectra are extremely rich, especially in terms of molecular line transitions.

HIFI data have also allowed a very detailed description of the young PN NGC 7027. Santander-Garcia *et al.* (2012) also used `Shapemol` for radiative transfer, spatio-kinematic modeling of the molecular envelope of the young planetary nebula NGC 7027 in several high- and low-J ^{12}CO and ^{13}CO transitions observed by HIFI and the IRAM 30 m radio telescope, and discussed the structure and dynamics of the molecular envelope. They used this code to build a Russian doll model to account for the physical and excitation conditions of the molecular envelope of NGC 7027. The model nebula consisted of four nested, mildly bipolar shells plus a pair of high-velocity blobs. The innermost shell is the thinnest and showed a significant increase in physical conditions (temperature, density, abundance, and velocity) compared to the adjacent shell. This is a clear indication of a shock front in the system, which may have played a role in shaping the nebula. Each of the high-velocity blobs is divided into two sections with considerably different physical conditions. The striking presence of H_2O in NGC 7027, a C-rich nebula, is likely due to photo-induced chemistry from the hot central star, although formation of water by shocks cannot be ruled out.

https://doi.org/10.1017/S1743921317001971 Published online by Cambridge University Press

6. Outlook

Soon, the THROES atlas (Garcia-Lario *et al.* 2016, this volume) will be publicly available through the Herschel science archive. THROES is a catalogue of fully reprocessed, homogenously reduced PACS spectra of all evolved stars from the AGB to the PN stage, including some massive red supergiants and LBVs, complemented with ancillary data taken by other facilities. SPIRE spectra will be added later. The catalog will contain more than 200 sources, originally part of more than 40 different research programs. This will hopefully trigger additional research by the community.

A lot of Herschel observations of PNe are available to be exploited and more interesting, scientific results await discovery.

Acknowledgements

I thank the SOC for inviting me to do this review talk. I am indebted to my colleagues of the MESS and HerPlanS consortia who have closely collaborated with her on the Herschel data. G. Van de Steene wishes to acknowledge support from FWO through travel grant K1C8716N. G. Van de Steene and the MESS consortium wish to acknowledge support from the Belgian Science Policy office through the ESA PRODEX programme.

References

Aleman, I., Ueta, T., & Ladjal, D., 2014, *A&A*, 566, A79
Bachiller, R., Huggins, P. J., Cox, P., Forveille, T., 1993, *A&A*, 267, 177
Bujarrabal, V., Alcolea, J., Soria-Ruiz, R., *et al.*, 2012, *A&A*, 537, A8
Blommaert, J. A. D. L., de Vries, B. L.,Waters, L. B. F. M., *et al.*, 2014, *A&A*, 565, A109
Boudet, N., Mutschke, H., Nayral, C., *et al.*, 2005, *ApJ.*, 633, 272
Cox N. L. J., Kerschbaum F., van Marle A.-J. *et al.*, 2012, *A&A*, 537, 35
de Graauw, T., Helmich, F. P., Phillips, T. G. *et al.*, 2010, *A&A*, 518, L4
Etxaluze, M., Cernicharo, J., Goicoechea, J. R., *et al.*, 2014, *A&A*, 566, A78
Goldsmith, P. F., 2001, *ApJ*, 557, 736
Griffin, M. J., Abergel, A., Abreu, A., *et al.*, 2010, *A&A*, 518, L3
Groenewegen, M. A. T., Waelkens, C., Barlow, M. J., *et al.*, 2011, *A&A*, 526, A162
Kastner, J. H., Montez, R., Jr., Balick, B., *et al.*, 2012, *AJ*, 144, 58
Mennella, V., Colangeli, L., & Bussoletti, E., 1995, *A&A*, 295, 165
Santander-Garcia M., Bujarrabal V., Alcolea J., 2012, *A&A*, 545, 114
Santander-Garcia M., Bujarrabal V., Koning N., Steffen W., 2015, *A&A*, 573, 56
Schwarz, H. E. & Monteiro, H., 2006, *ApJ*, 648, 430
Soria-Ruiz R., Bujarrabal V., Alcolea J., 2013, *A&A*, 559, 45
Steffen W. & Lopez J. A., 2006 *Rev. Mexicana AyA* 26 30
Steffen W., Koning N., Wenger S., Morisset C. and Magnor M., 2011, *IEEE Transactions on visualisation and computer graphics*, 17, 454
Pilbratt, G. L., Riedinger, J. R., Passvogel, T., *et al.*, 2010, *A&A*, 518, L1
Poglitsch, A., Waelkens, C., Geis, N., *et al.*, 2010, *A&A*, 518, L2
Ueta, T., Ladjal, D., Exter, K. M., *et al.*, 2014, *A&A*, 565, A36
Van de Steene G. C., van Hoof P. A. M., Exter K. M., *et al.*, 2015, *A&A*, 574, 134
van Hoof, P. A. M., Van de Steene, G. C., Barlow, M. J., *et al.*, 2010, *A&A*, 518, L137
van Hoof, P. A. M., Barlow, M. J., Van de Steene, G. C., *et al.*, 2012, *IAU Symp.*, 283, 41
van Hoof, P. A. M., Van de Steene, G. C., Exter, K. M., *et al.*, 2013, *A&A*, 560, A7
van Marle A. J., Cox N. L. J., Decin L., 2014, *A&A*, 570, 131
Zack, L. N. & Ziurys, L. M., 2013, *ApJ*, 765, 112
Zeigler, N. R., Zack, L. N., Woolf, N. J., & Ziurys, L. M., 2013, *ApJ*, 778, 16